JTTEE5 9:59-67

Development of Refractory Silicate-Yttria-Stabilized Zirconia Dual-Layer Thermal Barrier Coatings

Yirong He, Kang N. Lee, Surendra Tewari, and Robert A. Miller

(Submitted 20 December 1998; in revised form 5 December 1999)

Development of advanced thermal barrier coatings (TBCs) is the most promising approach for increasing the efficiency and performance of gas turbine engines by enhancing the temperature capability of hot section metallic components. Spallation of the yttria-stabilized zirconia (YSZ) top coat, induced by the oxidation of the bond coat coupled with the thermal expansion mismatch strain, is considered to be the ultimate failure mode for current state-of-the-art TBCs. Enhanced oxidation resistance of TBCs can be achieved by reducing the oxygen conductance of TBCs below that of thermally grown oxide (TGO) alumina scale. One approach is incorporating an oxygen barrier having an oxygen conductance lower than that of alumina scale. Mullite, rare earth silicates, and glass ceramics have been selected as potential candidates for the oxygen barrier. This paper presents the results of cyclic oxidation studies of oxygen barrier/YSZ dual-layer TBCs.

Keywords TBC, mullite, silicates, oxygen barrier, APS, sputtering, small particle plasma spray

1. Introduction

Thermal barrier coatings (TBCs) will play an essential role in the development of a new generation of land-based gas turbine systems with higher efficiency, longer lifetime, and lower cost.[1] Current state-of-the-art TBCs typically consist of a metallic bond coat and an yttria-stabilized zirconia (YSZ) top coat. Studies have shown that oxidation of the bond coat is primarily responsible for the failure of the current state-of-the-art TBCs.[2,3] This implies that the performance of TBCs can be improved by reducing the oxidation rate of the bond coat and/or by enhancing the adhesion of the thermally grown oxide (TGO). Based on this idea, much research has been carried out to understand the factors that affect the oxidation kinetics and alumina scale adhesion.[4,5,6] Pint *et al.* investigated the important factors for achieving an adherent Al_2O_3 scale in commercial TBC systems. An electron beam-physical vapor deposited (EB-PVD) YSZ coating on a bulk β-NiAl + Zr alloy showed a lifetime increased by a factor of 5 compared to a standard Pt aluminide/EB-PVD YSZ on Rene N5 (GE Aircraft Engines, Cincinnati OH).[6] The increased lifetime was attributed to improved scale adhesion. Sun *et al.*[7] and Schmitt-Thomas *et al.*[8] investigated a sealing concept by applying an intermediate Al_2O_3 diffusion barrier between the bond coat and the top YSZ coat. The thermal cyclic life at 100 °C with an Al_2O_3 intermediate layer was improved by a factor of 2 to 4.[7,8]

Chang *et al.*[9] and Phucharoen[10] used a finite element model to quantify the nature of the stress buildups in plasma-sprayed YSZ TBCs with an idealized sinusoidally rough interface between the ceramic and bond coat during a single cooling cycle. Thermal expansion mismatch generated tensile radial stresses in combination with compressive in-plane stresses in the YSZ near the tip of the peaks and compressive stresses in the valley region. In contrast, oxidation produced tensile stresses in the valleys and compressive stresses in the peak regions. Freborg *et al.* included bond coat and top coat creep and multiple thermal cycles in their finite element model to characterize the stresses in plasma-sprayed YSZ TBCs.[11] Their results indicated that top coat and bond coat creep also contributed to the generation of tensile stresses at the bond coat peak and off-peak locations and compressive stresses in the valley regions. Thus, the suggested evolution of residual stresses in plasma-sprayed TBCs is as follows. Early cracking at the bond coat peak is due to thermal expansion mismatch and creep, because thermal expansion mismatch and creep produce tension in the peak region and compression in the valley region. These cracks do not propagate due to the compressive stresses over the valley region. With the increase in the number of cycles and TGO thickness, the stresses over the valley become increasingly tensile. When the tensile stresses over the valley region are high enough to sustain the crack growth, the cracks at the peak link together and delamination occurs. Thus, the growth of TGO accelerates the TBC failure. Cheng and his colleagues[12] have used elastic-plastic finite element analysis to compute the thermal/residual stresses in a disk-shaped test specimen consisting of an EB-PVD YSZ TBC on Pt-Al bond coat and Ni-based superalloy substrate. Actual interface geometry was used to generate finite element models. It was found that the largest stress occurred in the TGO layer. Irregular interfaces lead to large vertical tensile stresses in the TGO.

It is believed that improved oxidation resistance of TBCs can be achieved by incorporating an oxygen barrier having an oxygen conductance lower than that of TGO alumina between the top YSZ coat and the bond coat. Rare earth silicates, such as La_2SiO_5, Sm_2SiO_5, and Y_2SiO_5, and glass ceramics, such as calcia-alumina-silicate (CAS), baria-alumina-silicate (BAS), and mullite, are promising as an oxygen barrier because of their low oxygen conductivity.

Yirong He, **Kang N. Lee,** and **Surendra Tewari,** Cleveland State University, Cleveland, OH 44115; and **Robert A. Miller,** NASA Glenn Research Center, Cleveland, OH 44135.

High velocity oxygen fuel (HVOF) thermal spraying, a new variant in thermal spray technology, exhibits the following advantages: (1) the high particle velocity renders a dense coating with higher adhesive and cohesive strength than its plasma-sprayed counterpart; (2) HVOF sprayed coatings have low surface roughness; and (3) less thermally induced changes are generated in the coating material compared to plasma-sprayed coating.[13,14] This technology has been used in spraying MCrAlY coating,[15] carbide coating,[14] and YSZ coating[16]. In this study, HVOF, air plasma spray (APS), sputtering, and small particle plasma spray (SPPS, Northwestern University, Evanston, IL) were used to apply the oxygen barrier coatings. This paper summarizes the preliminary results of the development of oxygen barrier coatings.

2. Experimental Procedure

Plasma spray grade powders of BAS, CAS, Y_2SiO_5, La_2SiO_5, and Sm_2SiO_5 were processed by commercial vendors (Zirtech, Niagara Fall, NY and MO-SCI Corporation, Rolla, MO). Plasma spray grade mullite powder (50 to 100 μm particle size) was purchased from Cerac (Milwaukee, WI). Submicron mullite powders for SPPS were purchased from Baikowski International (Charlotte, NC). A mullite target for sputtering was fabricated at Target Materials Inc. (Columbus, OH).

The standard TBCs in this study consisted of a 0.25 mm thick ZrO_2-8 wt.%Y_2O_3 (YSZ) top coat and 0.15 mm thick Ni-36Cr-6Al-0.5Y bond coat on grit-blasted CMSX4 + Y substrate (25 mm in diameter and 3 mm in thickness). The YSZ top coat was deposited using APS. Low pressure plasma spray was used to apply the bond coat. All coatings were sprayed on one face of the substrates.

The HVOF and APS were used to apply thick (50 to 75 μm) oxygen barrier coatings. Table 1 lists the HVOF and APS spray parameters for oxygen barrier coatings. Thin (1 to 10 μm) oxygen barrier coatings were deposited by sputtering and SPPS.

As-sprayed coupons were annealed at 1100 to 1150 °C in Ar-5%H_2 for 4 h. Thermal cyclic testing was performed at 1100 to 1150 °C using box furnaces or automated cyclic furnaces. Three cycling conditions were selected for the oxidation test: 1 h cycle (1 h high temperature-15 min room temperature), 20 h cycle (20 h high temperature-20 min room temperature), and 100 h cycle (100 h high temperature-20 min room temperature). Typically, samples reached the high temperature within 2 min and the low temperature within 5 min in each cycle.

X-ray diffractometry (XRD) was used to identify the phases present in the coating. Surface morphology and cross sections of the coating were examined using scanning electron microscopy equipped with an energy dispersive spectrometry attachment.

3. Results and Discussion

3.1 Selection of Oxygen Barrier

Low oxygen conductivity, chemical compatibility, and high coefficient of thermal expansion (CTE) were the three key factors in determining the selection of new ceramic materials. Since few ceramics meet all three requirements, some low CTE ceramics were selected as long as they met the other two criteria. The CTEs of the substrate, bond coat, Al_2O_3, and the selected materials are listed in Table 2. X-ray diffraction was used to identify the phases in as-received powders, and the results are listed in Table 3.

3.2 Development of Coating Application Technology

A previous study[17] indicated that refractory silicates and glass ceramics have the tendency to form amorphous or metastable phases, which are unstable at high temperatures, and phase transformations to stable phases take place under thermal exposure. In many cases, these phase transformations are detrimental to the integrity of the coating due to the large volume changes accompanying the transformations.[17,18] Heating the substrate above the phase transformation temperature suppressed the precipitation of amorphous or metastable phases and substantially enhanced the durability of silicate coatings.[17] Thus, the selected coatings were applied onto heated (1100 °C) substrates to investigate the effect of substrate temperature on the phase stability and the durability of TBCs.

Due to the relatively high surface roughness of conventional APS and HVOF coatings, it was not possible to deposit a thin oxygen barrier (<25 μm) with a complete coverage. Therefore, sputtering and SPPS were used to apply thin oxygen barrier coatings (1 to 10 μm).

3.3 Testing and Data Analysis

Standard YSZ Coating. Fig. 1(a) shows the cross section of as-sprayed standard YSZ. This coating failed after 9 cycles of 100 h cycle test at 1100 °C and 11 and 17 cycles of 20 h cycle test at 1100 °C. At 1150 °C, the coating failed after 10 to 18 cycles of 20 h cycle test and 130 cycles of 1 h cycle test. Fig. 1(b) represents a typical cross section of a standard YSZ coating after

Table 1 HVOF and APS spraying parameters for oxygen barrier coatings

			HVOF			
Torch	**Oxygen flow**	**Propylene flow**	**Air flow**	**Powder feed rate**	**Stand-off distance**	**Powder feed rate**
Diamond jet hybrid	606 SCFH(a)	167 SCFH	536 SCFH	35 g/min	25.4 cm	50 cm/s
			APS			
Powder particle size	**Gun power**	**Plasma gas flow(b)**	**Carrier gas flow**	**Powder feed rate**	**Stand-off distance**	**Traverse speed**
–200 mesh	45 kW	14.4SLPM Ar/9.6 SLPM He	6 SLPM	15 g/min	15 cm	30 cm/s

(a) Standard cubic foot per hour. (b) Standard liter per minute.

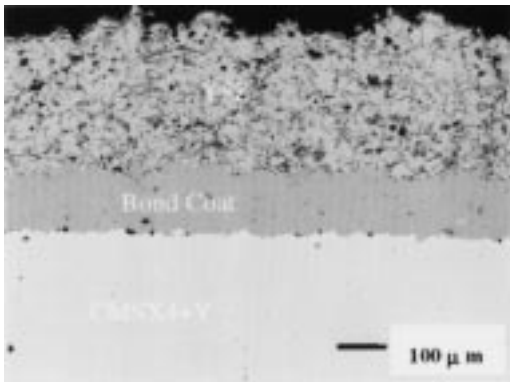

(a)

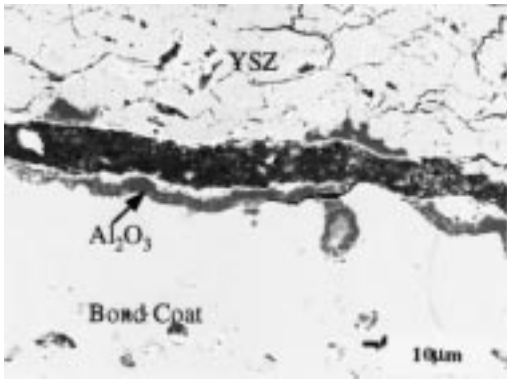

(b)

Fig. 1 (a) As-sprayed standard YSZ. (b) Standard YSZ after 18 to 20 h cycles at 1150 °C. Failure occurred mostly in YSZ near the YSZ/TGO boundary.

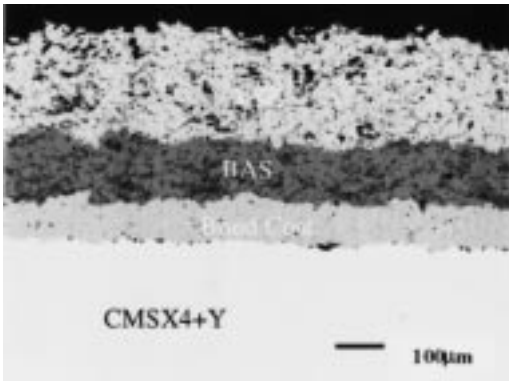

(a)

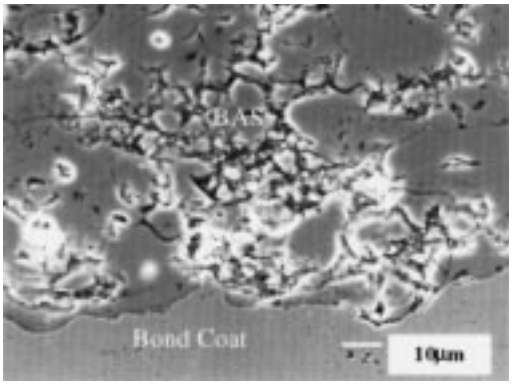

(b)

Fig. 2 As-sprayed HVOF BAS/YSZ. BAS coating is porous and incompletely melted. (a) Low magnification image. (b) High magnification image.

Table 2 CTEs of CMSX4 + Y, NiCrAlY, Al_2O_3, Selected ceramics and YSZ

Material	CMSX4 + Y	NiCrAlY	Al_2O_3	BAS, CAS, mullite	Y_2SiO_5	La_2SiO_5, Sm_2SiO_5	YSZ
CTE (10^{-6}/°C)	14–16	12–16	8–9	3–5	7–8	9–12	10

Table 3 XRD results of as-received powders

Powder	BAS	CAS	Mullite	Y_2SiO_5	La_2SiO_5	Sm_2SiO_5
Phase	Celsian	Anorthite	Mullite	Y_2SiO_5	La_2SiO_5 + La_2O_3 (minor)	Sm_2SiO_5

failure. Delamination was observed mainly within the YSZ top coat near the YSZ/TGO interface, while some occurred along the TGO/bond coat interface.

Thick Oxygen Barrier Coating (50 to 75 μm). *BAS Coating:* HVOF-sprayed BAS/YSZ coatings debonded after annealing. The debonded interface was powdery. Cross-sectional examination (Fig. 2) revealed that the BAS coating was porous and incompletely melted. Fig. 3(a) shows the cross section of as-sprayed APS BAS/YSZ coating. It has a layered structure, especially toward the BAS/bond coat interface. The APS BAS/YSZ coating survived the annealing, but failed after 2 cycles of 20 h cycle test at 1150 °C. The failure occurred mainly along the BAS/YSZ interface, as shown in Fig. 3(b).

Mullite Coating: As-sprayed HVOF mullite/YSZ coating showed a partial delamination at the mullite/bond coat interface and completely failed after a 1150 °C/4 h anneal.

The APS mullite coatings were applied on both heated (1100 °C) and unheated substrates to investigate the effect of substrate temperature on the phase stability and the coating performance. Mullite was the only phase detected on as-sprayed coupons (heated and unheated). The APS mullite coatings were dense with or without the substrate heating. Fig. 4(a) shows an as-sprayed APS mullite/YSZ without substrate heating. This coating failed after 1 cycle of 20 h cycle test at 1150 °C. Branching cracks formed and propagated in the mullite coating, as shown in Fig. 4(b). It is believed that the amorphous mullite and

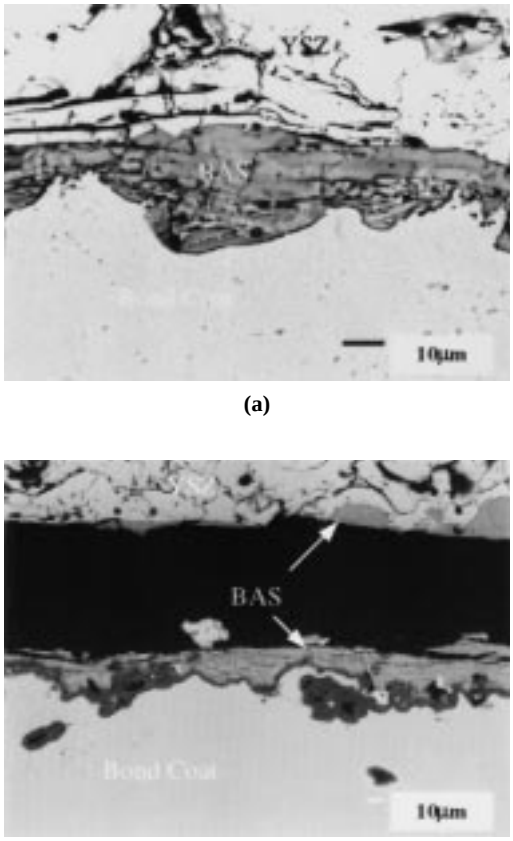

Fig. 3 (a) As-sprayed APS BAS/YSZ. BAS coating has a layered structure. (b) APS BAS/YSZ failed after 2 to 20 h cycles at 1150 °C. Failure occurred along the BAS/YSZ interface.

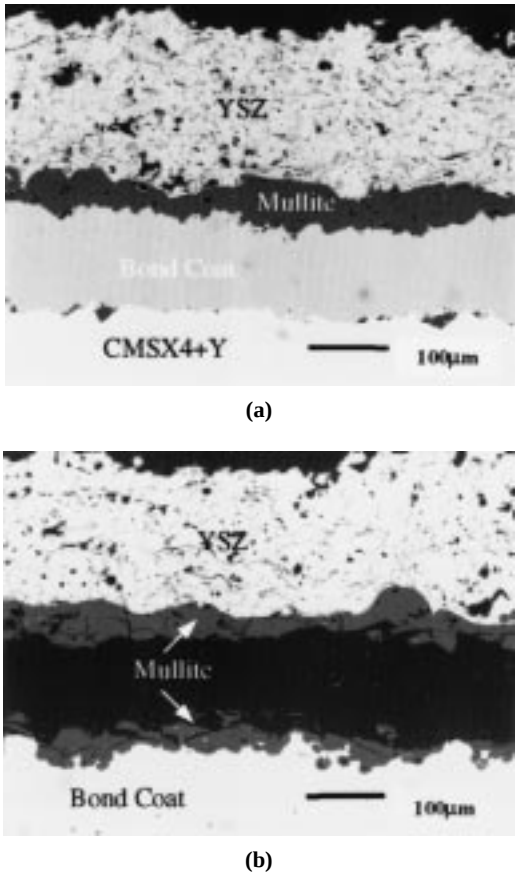

Fig. 4 (a) As-sprayed APS mullite/YSZ. (b) APS mullite/YSZ failed after 1 to 20 h cycles at 1150 °C. Mullite coating cracked and failure occurred inside the mullite coating.

the metastable alumina formed during the spraying and subsequently transformed to stable phases during the thermal cycling, causing the cracking. Trace amounts of SiO_2 and Al_2O_3 were detected by XRD in the mullite coating after 1 cycle of 20 h cycle test at 1150 °C. The mullite/YSZ coating applied on a heated substrate failed along the YSZ/mullite interface after annealing, indicating that the substrate heating did not lead to improved adhesion.

The premature failure of low CTE oxygen barrier coatings (BAS and mullite) is presumably due to stresses caused by their large CTE mismatch with the YSZ. Phase instability and the high Young's modulus of these coatings due to their high density are the other contributing factors to the stress. Applying a thin, low CTE coating may alleviate this problem because thinner coatings are more compliant.

Rare Earth Silicate Coatings (Y_2SiO_5, La_2SiO_5, Sm_2SiO_5): HVOF-sprayed rare earth silicate coatings were porous and incompletely melted, as shown in Fig. 5(a). This resulted in the failure of the coatings after annealing or 1 cycle of 20 h cycle test at 1150 °C. The APS coatings were denser, but cracks were observed in the as-sprayed coating, as shown in Fig. 5(b) The APS La_2SiO_5/YSZ coatings failed after 2 cycles of 20 h cycle test at 1150 °C.

Fig. 6(a) shows a cross section of as-sprayed APS Sm_2SiO_5 coating on heated substrate (1100 °C). These coatings tended to develop large cracks parallel to the YSZ/Sm_2SiO_5 coating interface and failed along the crack after annealing. Fig. 6(b) is a cross section of as-sprayed APS Sm_2SiO_5 coating on unheated substrate. Branching cracks formed in the coating. This coating failed within the Sm_2SiO_5 coating after 3 cycles of 20 h cycle test at 1150 °C. Fig. 6(c) and (d) show the cross sections of APS Sm_2SiO_5 coating on unheated substrate after the failure.

One key observation with these rare earth silicate coatings is that they cracked and failed prematurely despite the better CTE match. Also, substrate heating did not provide any improvement. The low thermal cycling resistance of rare earth silicate coatings may be due to their phase instability. X-ray diffraction analysis was performed on Y_2SiO_5, La_2SiO_5, and Sm_2SiO_5 coatings to study the phase stability of these coatings. The results for La_2SiO_5 are listed in Table 4. Y_2SiO_5 and Sm_2SiO_5 showed a similar behavior. The as-sprayed La_2SiO_5 coating deposited on an unheated substrate was amorphous, whereas the single-phase La_2O_3 was deposited when sprayed on a heated substrate. Both as-sprayed coatings transformed to $La_2SiO_5 + La_2O_3$ after annealing. After 5 cycles, the $LaAlO_3$ phase appeared, presumably formed by the reaction between La_2O_3 and Al_2O_3. The low thermal shock resistance of the La_2SiO_5 coating was presumably due to stresses generated by the phase transformations and the CTE mismatch between the La_2SiO_5 and La_2O_3 that coexisted in the coating.

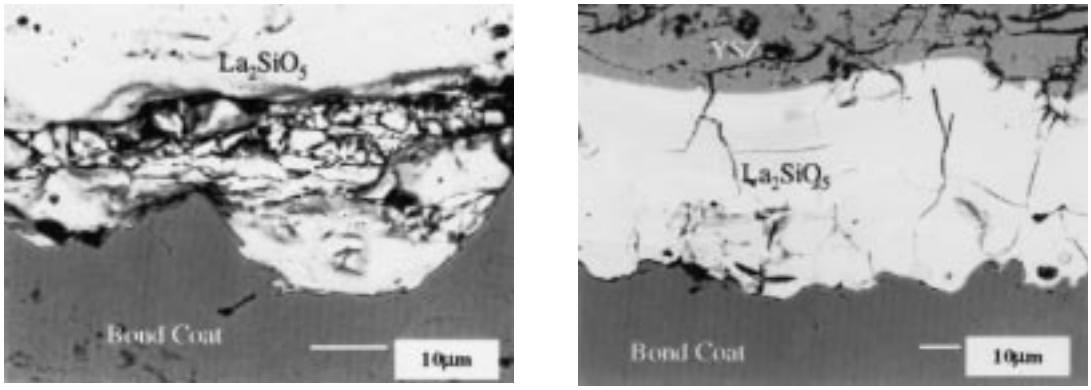

(a) **(b)**

Fig. 5 (a) As-sprayed HVOF La_2SiO_5/YSZ. La_2SiO_5 coating is porous and incompletely melted. (b) As-sprayed APS La_2SiO_5/YSZ. La_2SiO_5 coating is denser but cracked.

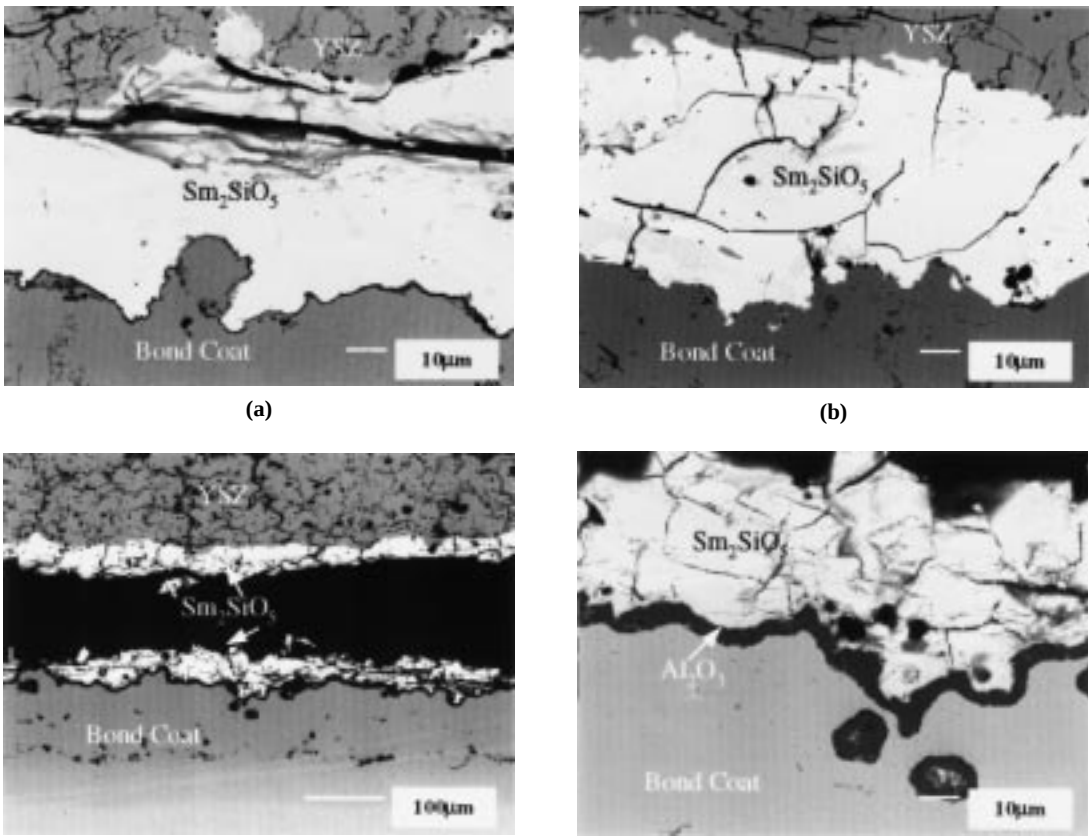

(a) **(b)**

(c) **(d)**

Fig. 6 (a) As-sprayed APS Sm_2SiO_5/YSZ on heated substrate. Large cracks developed in the Sm_2SiO_5 coating. (b) As-sprayed APS Sm_2SiO_5/YSZ on unheated substrate. Microcracks developed in the Sm_2SiO_5 coating. (c) APS Sm_2SiO_5/YSZ on unheated substrate after 3 to 20 h cycles at 1150 °C. Failure occurred in the Sm_2SiO_5 coating. (d) High magnification image of (c). More cracks developed in the Sm_2SiO_5.

Heat treatments were performed on La_2SiO_5 powder to further investigate the phase stability. Powder was processed by fusion and grinding. Both as-solidified and ground La_2SiO_5 contained a significant amount of La_2O_3, indicating some La_2SiO_5 decomposed to $La_2O_3 + SiO_2$ (amorphous) during the solidification. On heating, most of the La_2O_3 and SiO_2 readily reassociated to La_2SiO_5. A similar phenomenon was reported for $ZrSiO_4$.[19] The cooling rate (furnace cooling versus air cooling) did not affect the phase transformation behavior of La_2SiO_5. A 1 mm thick APS La_2SiO_5 stand-alone sample was obtained by spraying La_2SiO_5 onto a graphite plate and subsequently burning off the graphite at 660 °C in air. The coupon was annealed in Ar-5%H_2 for 4 h at 1100 °C before undergoing the 3 cycles of 20 h cycle test at 1150 °C. The results of XRD are shown in Table 4. La_2SiO_5 and La_2O_3 were the major phases after the graphite burn-off and annealing. After 3 cycles

of 20 h cycle test at 1150 °C, most La_2O_3 reassociated to La_2SiO_5, similar to the behavior of La_2SiO_5 powder. The difference between the La_2SiO_5 coating and the bulk La_2SiO_5 was that the La_2SiO_5 coating retained a substantial amount of La_2O_3 after thermal exposure.

Table 4 Summary of XRD results of La_2SiO_5

Coupon	Heat treatment condition	XRD results
La_2SiO_5 heated	APS sprayed	La_2O_3
	Annealed(a)	$La_2SiO_5 + La_2O_3$
	1 cycle(b)	$La_2SiO_5 + La_2O_3$
	5 cycles	$LaAlO_3 + \alpha$–Al_2O_3 + La_2SiO_5
	10 cycles	α-Al_2O_3 + $LaAlO_3$ + $NiAl_2O_4$ + $LaAlSi_2O_6$
La_2SiO_5 unheated	APS sprayed	Amorphous
	Annealed	$La_2SiO_5 + La_2O_3$
	2 cycles	$La_2SiO_5 + La_2O_3$
La_2SiO_5 powder	As received (–140/+200)	La_2SiO_5, La_2O_3 (both major)
	1150 °C/4 h	$La_2SiO_5 + La_2O_3$ (minor)
	1150 °C/20 h	$La_2SiO_5 + La_2O_3$ (minor)
	1200 °C/1 h	$La_2SiO_5 + La_2O_3$ (minor)
	1200 °C/24 h	$La_2SiO_5 + La_2O_3$ (minor)
	1300 °C/24 h in air	La_2SiO_5
	1400 °C/24 h in air	La_2SiO_5
	1500 °C/1 h	$La_2SiO_5 + La_2O_3$ (very minor)
	1500 °C/24 h	La_2SiO_5
Powder after 1300 °C/24 h in air	1150 °C/20 h, air quench	La_2SiO_5
	1150 °C/20 h, furnace cooling	La_2SiO_5
APS La_2SiO_5 stand alone	660 °C/6 h to burn out graphite substrate	$La_2SiO_5 + La_2O_3$
	Annealed at 1100 °C/4 h	$La_2SiO_5 + La_2O_3$
	1150 °C/20 h, 3 cycles	$La_2SiO_5 + La_2O_3$ (very minor)

(a) Annealing condition: 1150 °C/4 h in Ar-5%H_2 (b) Cyclic test condition: 1150 °C/20 h cycle (20 h high temperature, 20 min room temperature) in air

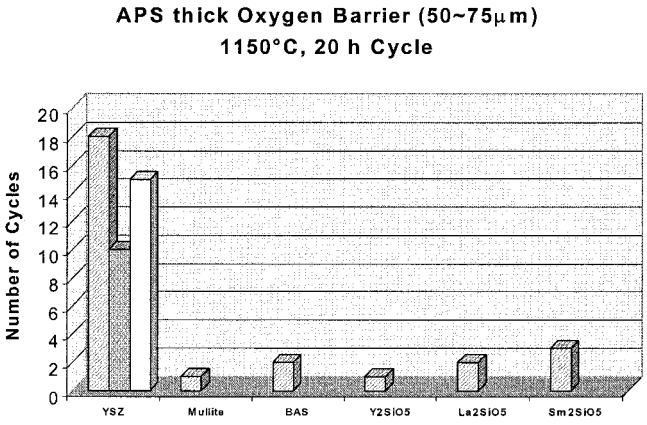

Fig. 7 Cyclic oxidation durability of thick APS oxygen barrier/YSZ TBCs. Each bar represents one tested specimen.

Fig. 7 summarizes the cyclic oxidation durability of APS thick oxygen barrier/YSZ TBCs. All TBCs with thick oxygen barrier were inferior to the standard YSZ. The three bars for standard YSZ in Fig 7 represent the data for three coupons from three different batches.

Thin Oxygen Barrier Coating (1 to 10 μm). Fig. 8 is a cross section of sputtered 3 μm mullite/YSZ TBC after 8 cycles of 20 h cycle test at 1100 °C. A dense layer of TGO Al_2O_3 formed underneath the continuous mullite layer. Cracks formed in the YSZ near the mullite/YSZ interface and debonding was observed at the valley of the mullite/YSZ interface. Failure occurred mostly in the YSZ near the YSZ/mullite interface (Fig. 8b), similar to the failure mode of standard TBCs. Sputtered 6 μm mullite/YSZ showed a similar behavior to the 3 μm mullite/YSZ. Fig. 9 shows the X-ray map for A1, Si, and O for the cross section of sputtered 6 μm mullite/YSZ after failure (13 cycles of 20 h cycle test at 1100 °C), showing the TGO Al_2O_3 underneath the mullite. The thickness of TGO alumina was reduced by a factor of 2 in the presence of the thin mullite oxygen barrier (Fig. 10).

Fig. 11 shows the cross section of as-sprayed SPPS mullite coating. The bond coat was completely covered by the mullite coating; however, the coating thickness was not uniform. Further optimization is necessary to produce a uniform coating. The

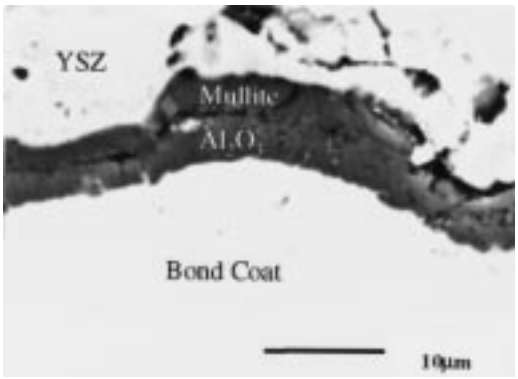

(a)

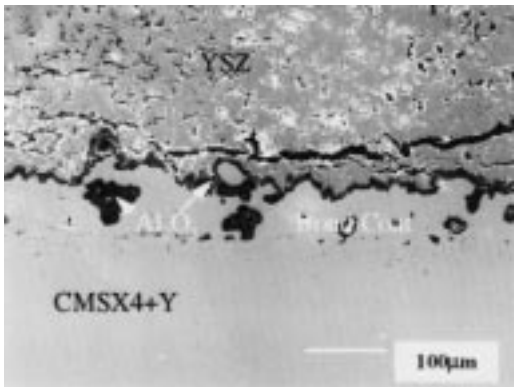

(b)

Fig. 8 (a) Cross section of 3 μm mullite/YSZ after 8 to 20 h cycles at 1100 °C. Dense Al_2O_3 formed underneath the mullite coating. (b) Low magnification image of (a)**.** Failure occurred in YSZ, similar to the failure mode of standard YSZ.

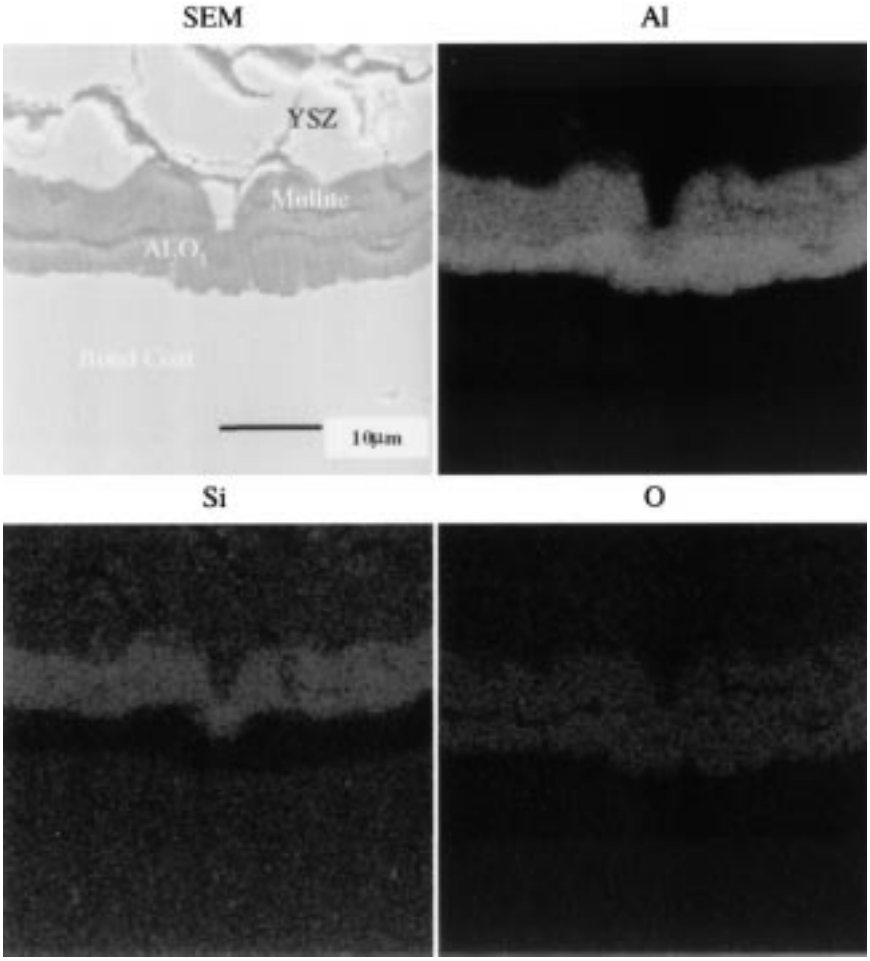

Fig. 9 Cross section and X-ray mapping for Al, Si, and O of 6 μm mullite/YSZ after 13 to 20 h cycles at 1100 °C.

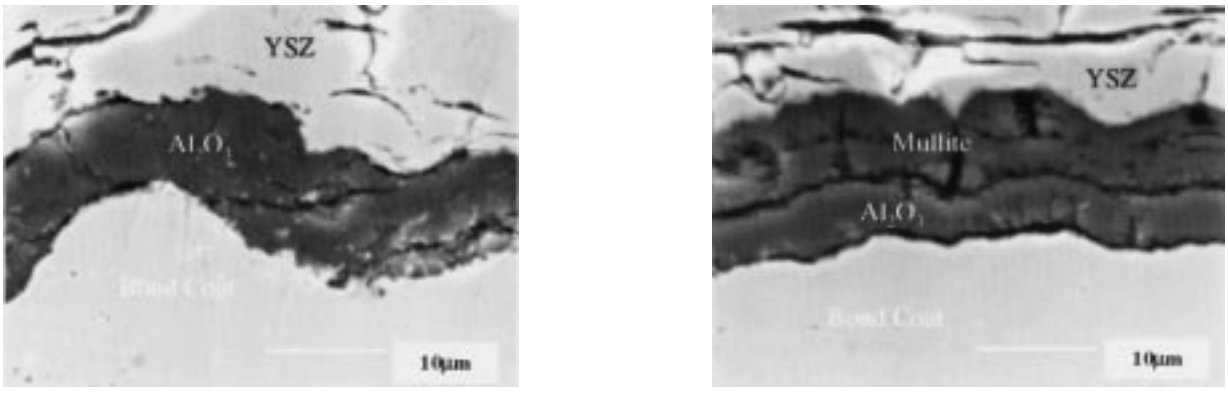

(a) **(b)**

Fig. 10 (a) Standard YSZ after 11 to 20 h cycles at 1100 °C. (b) 6 μm mullite/YSZ after 13 to 20 h cycles at 1100 °C. The thickness of Al_2O_3 is about one-half that formed in the standard YSZ.

SPPS mullite/YSZ failed after 8 cycles of 20 h cycle test and 5 cycles of 100 h cycle test at 1100 °C.

Figures 12 and 13 show the lifetime of TBCs with thin oxygen barrier in 20 h and 100 h cycle tests, respectively, at 1100 °C. Thin mullite/YSZ TBCs showed durability comparable to that of a standard TBC, demonstrating the potential of thin oxygen barrier coatings.

Even though the sputtered and SPPS thin mullite coatings performed far better than the thick APS mullite coatings with significantly reduced bond coat oxidation rates, there was no

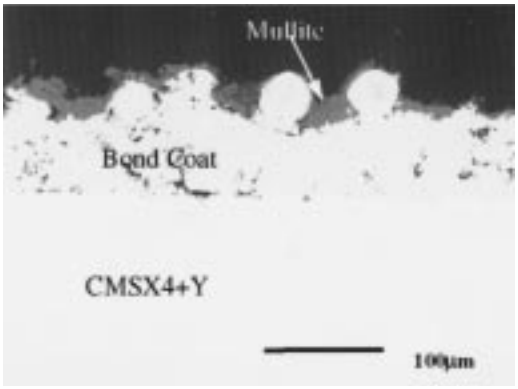

(a)

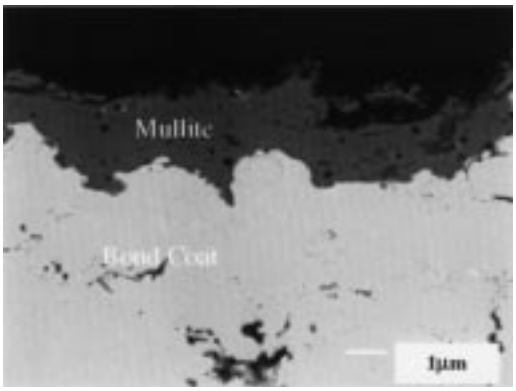

(b)

Fig. 11 (a) As-prayed SPPS mullite. Mullite completely covered the rough surface of the bond coat. (b) High magnification image of (a).

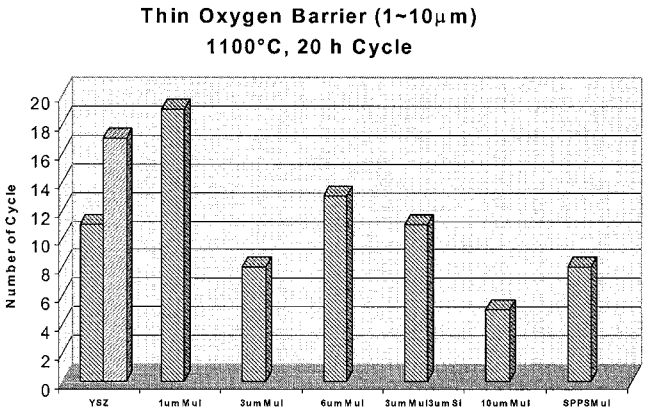

Fig. 12 20 h cyclic oxidation durability of thin oxygen barrier/YSZ TBCs at 1100 °C. Each bar represents one tested specimen.

improvement in the coating life compared to standard YSZ TBCs. It is interesting to note that at the time of failure, the combined thickness of mullite and TGO in the thin mullite/YSZ TBC (Fig. 10b) was about the same as the thickness of TGO in the standard TBC (Fig. 10a). It appears that the mullite coating, due to its low CTE and high Young's modulus, acted like TGO in generating tensile stresses. Thus, the mullite/YSZ TBC failed when the combined thickness of mullite + TGO reached the thickness of

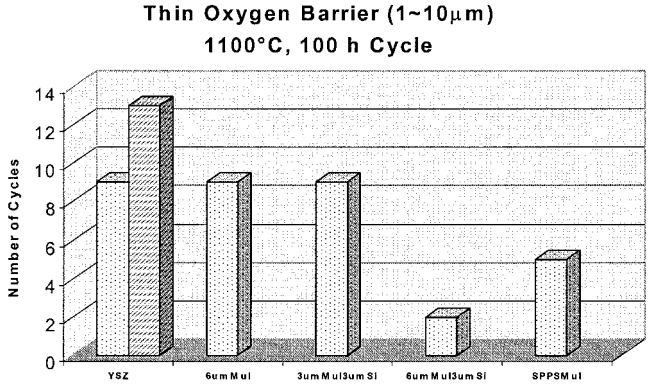

Fig. 13 100 h cyclic oxidation durability of thin oxygen barrier/YSZ TBCs at 1100 °C. Each bar represents one tested specimen.

TGO in the standard TBC at the time of failure. This indicates that a higher CTE and lower modulus are required for the oxygen barrier to minimize the stress generation by the oxygen barrier.

4. Summary and Conclusions

The HVOF-sprayed oxygen barrier coatings tended to be incompletely melted and powdery, while APS-sprayed oxygen barrier coatings were denser. As a result, the HVOF coatings were in general inferior to APS coatings.

The TBCs with a thick (50 to 75 μm), low CTE oxygen barrier coating (mullite, BAS, CAS) tended to delaminate within the oxygen barrier coating or at the YSZ/low CTE coating interface, presumably due to the CTE mismatch stress. This indicates the need for thin coatings to reduce the CTE mismatch stresses. Microcracks were observed in the APS-sprayed thick (50 to 75 μm) rare earth silicate coatings. On thermal cycling, the rare earth silicate coatings failed prematurely by developing more cracks. Phase instability appeared to be the major contributor to the lack of thermal shock resistance.

Thin mullite oxygen barrier coatings (1 to 10 μm) reduced the oxidation rate of the bond coat twofold. The durability of sputtered or SPPS thin mullite/YSZ TBCs was far better than that of thick APS mullite/YSZ TBCs. However, the life of the sputtered or SPPS mullite/YSZ TBCs was still similar to that of standard TBCs, suggesting that improved oxidation resistance alone was not sufficient for enhanced TBC durability. The low CTE and high elastic modulus of mullite appear to be responsible for the lack of lifetime improvement in thin mullite/YSZ TBCs. Future work will be focused on a thin oxygen barrier with high CTE and low modulus.

Acknowledgments

We are grateful to George Leissler and Gary Kostyak of Dynacs, NASA Glenn Group, for processing sprayed and sputtered coatings, respectively. We are also thankful to Northwestern University for the supply of SPPS coatings. This work was supported by the DOE AGTSR program under Contract No. 96-01-SR042.

References

1. W.P. Parks, E.E. Hoffman, W.Y. Lee, and I.G. Wright: *Proc. Thermal Barrier Coating Workshop,* NASA Conference Publication 3312, NASA, Washington, DC, 1995, pp. 35-47.

2. R.A. Miller and C.E. Lowell: *Thin Solid Films,* 1982, vol. 95, pp. 265-73.
3. R.A. Miller: *J. Am. Ceram. Soc.,* 1984,vol. 67, pp. 517-21.
4. R.A. Miller: *Proc. Thermal Barrier Coating Workshop,* NASA Conference Publication 3312, NASA, Washington, DC, 1995, pp. 17-34.
5. J. Schaeffer: *Proc. TBC Interagency Coordination Committee,* Cincinnati, OH, May 19-21, 1997, pp. 99-108.
6. B.A. Pint, I.G. Wright, W.Y. Lee, Y. Zhang, K. Pruβner, K.B. Alexander: *Mater. Sci. Eng.* 1998, vol. A245, pp. 201-11.
7. J. Sun, E. Chang, and B. Wu: *Mater. Trans. JIM,* 1993, vol. 34 (7), pp. 614-31.
8. K.G. Schmitt-Thomas, U. Dietl, and H. Haindl: *Ind. Ceram.,* 1996, vol. 16 (3), pp. 195-98.
9. G.C. Chang, W.A. Phucharoen, and R.A. Miller: *Surface Coating Technol.,* 1987, vol. 30, pp. 13-28.
10. W.A. Phucharoen: Ph.D. Dissertion, Cleveland State University, Cleveland, OH, 1990.
11. A.M. Freborg, B.L. Ferguson, W.J. Brindley, And G.J. Petrus: *Mater. Sci. Eng.,* 1998, vol. A245, pp. 182-90.
12. J. Cheng, E.H. Jordan, B. Barber, and M. Gell: *Acta Mater.,* 1998, vol. 46 (16), pp. 5839-50.
13. O.C. Brandt: *J. Thermal Spraying Technol.,* 1995, vol. 4 (2), pp. 147-52.
14. D. Lee: *J. Thermal Spray Technol.,* 1995, vol. 4 (3), pp. 229-34.
15. H. van Esch and W. Greaves: *Proc. Int. Gas Turbine and Aeroengine Congr. and Exhib.,* Birmingham, United Kingdom, June 10–13, ASME, New York, NY, 1996, pp. 1-5.
16. Advanced Materials and Processes: *Metallurgia,* 1995, vol. 62 (3), pp. 136.
17. K.N. Lee, R.A. Miller, and N.S. Jacobson: *J. Am. Ceram. Soc.,* 1995, vol. 78 (3), pp. 705-10.
18. G.N. Heintz and U. Uematsu: *Surface Coating Technol.,* 1992, vol. 50, pp. 213-22.
19. C.E. Curtis and H.G. Sowman: *J. Am. Ceram. Soc.,* vol. 36, 1953, pp. 190.